Precision measurement of the crossing between the $(J,M)=(2,2)$ and $(0,0)$ sublevels in $3\,^3P$ helium

Dong-Hai Yang and Harold Metcalf
Department of Physics, State University of New York, Stony Brook, New York 11794
(Received 27 March 1985)

We have measured the position of the magnetic field level crossing of the $J=2$, $M=2$, and the $J=M=0$ sublevels of the $3\,^3P$ state of helium. Time-resolved level-crossing spectroscopy, coupled with photoionization detection, were used to achieve accuracy of 1.5 ppm. The result, quoted in NMR frequency in water, is 9695.023(15) kHz, in good agreement with earlier, less precise measurements.

I. INTRODUCTION

Precision measurements of atomic-energy splittings in simple atoms have always been a subject of interest and importance for many reasons. First, atomic theory has been developed to such a high degree of accuracy and confidence that, coupled with precision measurements, it serves as an important source for values of fundamental constants. Second, it is important to conduct significant and stringent tests of such theories by making precision measurements of appropriate quantities. Third, many significant advances in physics arose because of small discrepancies revealed by precision measurements.

We report here the first results of a series of precision fine-structure measurements in the $3\,^3P$ states of helium. Preliminary results from a related experiment have been reported previously.[1] Although measurements of the fine structure in the $2\,^3P$ state of helium can now be compared with theory at the ppm level,[2] there is no theory that allows for comparably accurate comparison in the $3\,^3P$ state. This fine-structure interval has been measured in the past by Kaul,[3] Lhuillier *et al.*,[4] and Kramer and Pipkin;[5] the present work agrees well with these earlier but less-precise results.

Our work comprises a precision measurement of the magnetic field crossing point of the $J=2$, $M=2$, and $J=M=0$ sublevels of the $3\,^3P$ state of helium. The experimental technique is related to both quantum-beat and level-crossing spectroscopy, and may be appropriately called time-resolved level-crossing spectroscopy. Because it detects a quantum interference signal that is in many ways analogous to the one from Ramsey's separated oscillatory-fields method, it allows considerably higher precision than methods that are not time resolved.[6–8]

In this method, a pulse of laser light produces a superposition of atomic excited states that is allowed to evolve freely for a selectable time. Then the relative phase of the components of this superposition is detected. Details of the signal shape have been described previously,[6,7] and show that, for long delay times, this method can achieve signals narrower than the natural width. For our choice of parameters, the resulting signal is almost a cosine wave having many oscillations, instead of the single peak characteristic of ordinary spectroscopic signals. The fitting process is most sensitive to the location of the many inflection points and can yield higher precision than fitting a single peak. We use photoionization detection to enhance the signal, reduce background arising from light detection, and provide better geometric definition.

The precision of almost all spectroscopic measurements is ultimately dictated by the width of the signal, which is usually determined by the time spent in one of the two states involved in the transition under study. Often one of these states can decay, thereby limiting the observation time and broadening the signal. For example, the $3\,^3P$ state of helium under study in our experiment can decay to the $2\,^3S$ state ($\tau=98$ ns) thereby broadening the level to its natural width of 1.75 MHz, full width at half maximum (FWHM).

Observation of spectra with features narrower than the natural width can be accomplished by a number of time-resolved techniques. Among these are separated oscillatory fields, time-resolved observation of quantum beats, and time-resolved Mössbauer spectra. The basis of all these methods is the biased selection of that part of the signal obtained after the passage of a few natural lifetimes. Narrowing of signals by such time-resolved techniques always weakens the signal and usually reduces the signal-to-noise ratio as well, resulting in a loss of information. In general, there is nothing to be gained by discarding data as long as the information it carries is understood. But since we never have complete information about the signal shape, selective deletion of data by time resolution may be of great help. Certain general characteristics of spectroscopic signals narrowed to less than their natural widths have been presented previously.[6] In this experiment, a significant improvement in accuracy results from the use of time-delayed techniques. This particular aspect will be discussed in a separate paper that will be a sequel to Ref. 6.

The level-crossing field depends on both the zero-field fine structure and the Zeeman effect. The precise measurement reported here can be combined with an accurate evaluation of the Zeeman effect to determine the fine-structure splitting. This can be compared with the relativistic theory of the helium atom including the quantum-electrodynamic (QED) contribution for a test of that theory.

II. EXPERIMENTAL ARRANGEMENT

In our experiments, metastable $2\,^3S$ helium atoms in a beam are excited to the $3\,^3P$ state in a 0.227-T, dc magnetic field by a pulse of 389-nm light from a nitrogen-laser-pumped dye laser. Then they are allowed to evolve in the dark for times as long as 3.5 natural lifetimes, and finally are photoionized by a pulse of green light from a Nd:YAG (yttrium aluminum garnet) laser. We measure the magnetic field dependence of the resulting photocurrent while sweeping the field through about 7×10^{-4} T around the crossing point near 0.227 T. A run consists of accumulating the data from several such sweeps.

A. Atom source

The experimental arrangement is shown in Fig. 1. A pulsed valve,[9] triggered by a pulse of about 150 V, is used to admit a 400-μs pulse of helium gas from a high-pressure reservoir (about 5.5×10^5 Pa$=$75 psi) into the vacuum system through a 0.335-mm-diam orifice. Synchronized with the valve opening is a 40-kV pulsed discharge from a carefully placed wire about 5 mm away from the aperture that creates about $1{:}10^5$ of $2\,^3S$ metastables in the beam. After a skimmer and two apertures that separate differentially pumped chambers, the atoms fly freely for about 500 μs in a 10^{-6}-Torr beam line to the interaction region about 1.0 m away where there is a magnetic field of about 0.227 T. This source produces a pulse with peak density of about 10^5 metastables/cm^3 in the interaction region, and the effective volume of the laser beams selects some of those atoms.

B. Geometry and timing

At the interaction region the atomic beam is crossed by two pulsed laser beams, separated by an adjustable time interval. The first one is a 388.9-nm dye-laser beam pumped by a homemade nitrogen laser[10] (duration about 6 ns, spectral width about 3 GHz) that excites the metastables to the $3\,^3P$ state. After a chosen delay time (adjustable from 80 to 600 ns), an 8-ns-long, 532-nm green-light pulse, frequency doubled from a homemade Q-switched Nd:YAG laser,[11] ionizes the atoms from the $3\,^3P$ state,

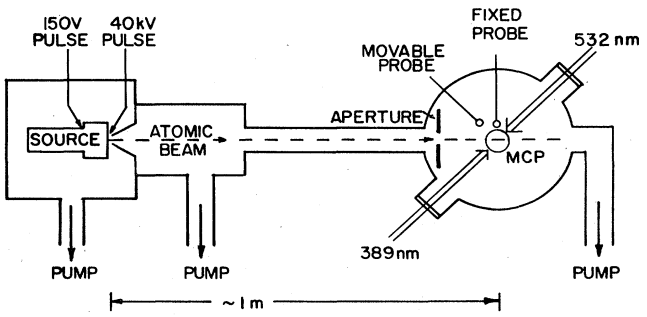

FIG. 1. Overall schematic diagram of apparatus. Atomic beam source is a pulsed valve as described in Ref. 9. Output of the MCP detector is fed to electronics as shown in Fig. 2. Two laser beams propagate in opposite directions for convenience. The fixed and movable NMR probes are discussed later.

creating photoelectrons. These two laser beams are well aligned to be nearly coincident (counterpropagating for convenience) and are both linearly polarized perpendicular to the magnetic field. The two laser beams cross the atomic beam at a 45° angle, and all three beams propagate in the plane perpendicular to the magnetic field.

C. Laser synchronization and tuning

In order to synchronize the pulsed lasers with each other and with the atomic beam pulse, we have built a digital, multichannel pulse generator based on a 10-MHz quartz oscillator (see Fig. 2). It first triggers the atomic beam valve and then the discharge, as well as starting the flashlamps in the Nd:YAG laser. After an appropriate (adjustable) flight time for the metastables it triggers the nitrogen laser for the 389-nm light (the Nd:YAG laser is triggered by the nitrogen laser through appropriate delay cables).

The peak of the velocity distribution of metastable atoms in the gas pulse is at about 2000 m/s so that the 389-nm laser pulse is set for a well-defined time about 500 μs after the source emits the gas pulse, and detuned by $\nu_D=(v/\lambda)\cos\theta=3.5$ GHz. Only atoms within a limited range of velocities selected by this time of flight are present at the interaction region, 1 m away, for excitation by the laser pulse. The 100-μs discharge duration determines a velocity range of about 400 m/s for these atoms, centered at about 2000 m/s. This corresponds to a Doppler-shifted frequency range of about 0.7 GHz, centered at about 3.5 GHz, so that a laser frequency drift of a few GHz moves the tuning well away from the peak of the velocity distribution. Few-GHz stability is somewhat difficult to achieve, so we deliberately overpump the dye-laser oscillator to broaden its spectral output by exciting several of its 400-MHz separated cavity modes. The result is light energy spread over a range of a few gigahertz, so that modest frequency drifts do not severely reduce the number of atoms that can be excited. The price for this is a small addition to the background.

The frequency of the 389-nm laser is first roughly set by observing the optogalvanic effect in a separate discharge cell made for this purpose. Then the laser is fine tuned by scanning its frequency and recording the YAG-laser-induced photocurrent at a fixed field near 0.227 T. The readily calculated spectrum is not simple because there are many fine-structure sublevels shifted by the Zeeman effect, and there are 12 allowed optical transitions among them. We compare the signal from the laser scan with the calculation (Fig. 3) in order to find the correct operating frequency for excitation of the levels of interest. This tuning process is repeated every few runs to correct for laser frequency shifts caused by changes in environmental conditions such as atmospheric pressure or room temperature, relaxation of mounts, etc.

The time delay between the two laser pulses must be held stable to within less than their duration. We use the high-voltage pulse from the nitrogen-laser discharge to trigger the Q switch of the Nd:YAG laser, and thus achieve a jitter of less than 5 ns (typically 1 or 2 ns).

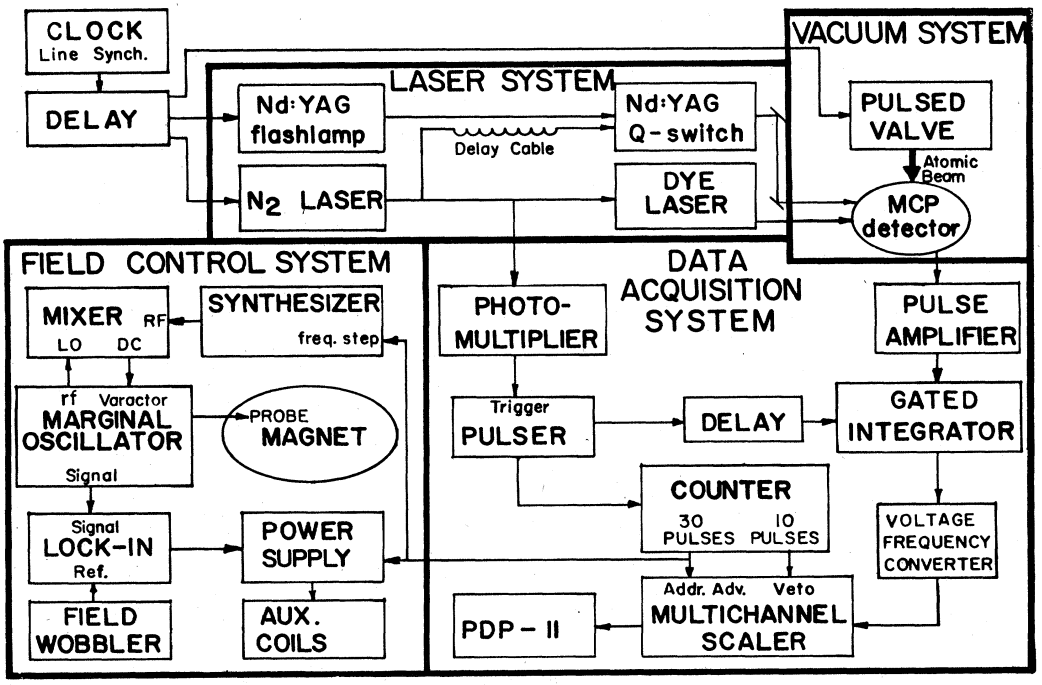

FIG. 2. Schematic diagram showing major system components of the apparatus. The different delays are accomplished by different channels of the multichannel delay generator.

D. Magnetic field

The highly homogeneous magnetic field is locked to and swept by an NMR system that is locked to a frequency synthesizer (Fig. 2). The synthesizer time base provides the ultimate accuracy for this experiment, and for that reason it is frequently checked with other time bases (its specification is 0.03-ppm drift).

We use a Walker/Magnion model L-128 laboratory electromagnet with 30-cm-diam pole pieces forming an 8-cm gap to produce our 0.227-T magnetic field. The magnet was carefully aligned and the pole pieces "ring shimmed" to optimize its homogeneity near 0.227 T. The field is locked to a marginal oscillator through a lock-in amplifier whose output drives an operational power supply that feeds an auxiliary set of trimming and sweep coils wound around the magnet pole pieces (see Fig. 2). The marginal oscillator frequency is locked to a Hewlett Packard frequency synthesizer through a mixer, varactor diode, and dc coupled amplifier (PAR 113). Thus the field is locked to the frequency of the sweepable synthesizer.

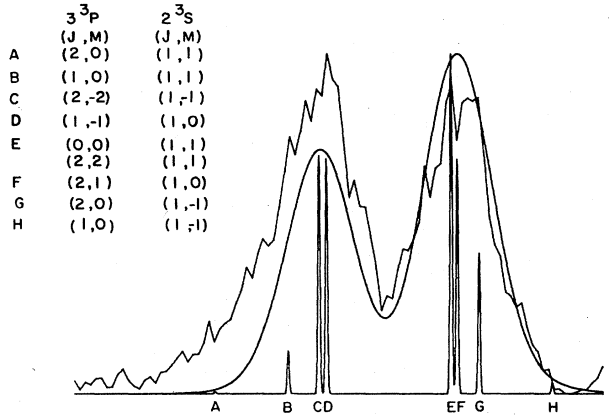

FIG. 3. Tuning scans showing calculated and measured spectra. The width in each case arises primarily from the laser width. Vertical lines show the strength and location of the optically allowed transitions. Line labeled E is the transition of interest.

The mineral-oil-filled NMR probe, used for both measuring and locking the magnetic field, is located about 7 cm from the center of the interaction region. There is another moveable NMR probe that can be inserted directly into the interaction region to measure the field difference between the interaction region and the location of the fixed probe. We measure this difference (with the field set at the center of the sweep) every few runs to avoid errors from drifts (which turn out to be small). The fixed probe is nearly spherical but the movable probe is cylindrical, with a length-to-diameter ratio of about 2:1. Our frequency, corrected for its diamagnetic shielding effect,[12] is $f(\text{corr}) = f(\text{meas}) - 1.4$ ppm.

E. Data acquisition

The photoelectrons are directed by a weak electric field (about 150 V/cm) into a pair of Varian microchannel plates (MCP) biased for moderate gain (see Fig. 4). These were chosen because they are relatively insensitive to a magnetic field when oriented perpendicular to it, and because they are very linear with a high saturation threshold.

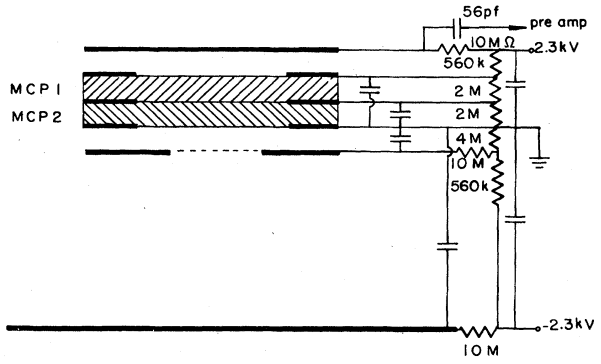

FIG. 4. Detector circuit showing MCP plates and bias voltages. Magnetic field is perpendicular to the plates. Unlabeled capacitors are 470 pF.

The signal from the MCP is amplified by standard NIM modules, and the pulse peak (sampled and held by a LeCroy 227) is presented to a Hewlett Packard 2211B voltage-to-frequency converter (VFC) as shown in Fig. 2. The 50—100-kHz VFC output from each laser pulse is counted for 50 ms by a homemade multichannel scalar, stored in its memory, and then the circuits are reset for the next laser pulse. The dwell at each value of field is 30 laser pulses or 4 s, but data from the first 10 of the laser pulses are vetoed to allow the field to settle after its step. At the end of a run the data is transferred to a PDP-11/23 computer for later analysis and fitting.

III. EXPERIMENTAL RESULTS AND DATA FITTING

The signals derived from time-resolved level crossing have been discussed in Refs. 1, 6, and 7, and the use of photoionization detection has been described by Luk *et al.*[13] The even part of the signal $R_e(B,T)$ at a fixed delay time T oscillates with field B according to Eq. (22) of Ref. 7;

$$R_e = C_0 + C_1 \frac{e^{-\Gamma T}}{(\Gamma^2+\omega^2)^2} \times \{(\omega^2-\Gamma^2)[\alpha\cos(\omega T)-\beta\sin(\omega T)] + 2\omega\Gamma[\alpha\sin(\omega T)+\beta\cos(\omega T)]\}\ , \quad (1)$$

where $1/\Gamma$ is the lifetime of the $3\,^3P$ state, $\hbar\omega=\hbar\omega(B)$ is the field-dependent energy separation between the levels of interest, T is the delay time between the laser pulses, and C_0 and C_1 are nearly-field-independent parameters containing various terms in the sum of Eq. (22) of Ref. 7. Here α and β are time-independent parameters given by[7]

$$\alpha = 1+e^{-\Gamma\tau}\cos(\omega\tau)-e^{-\Gamma\theta}\cos(\omega\theta)-e^{-\Gamma\delta}\cos(\omega\delta)\ , \quad (2a)$$

$$\beta = e^{-\Gamma\tau}\sin(\omega\tau)-e^{-\Gamma\theta}\sin(\omega\theta)-e^{-\Gamma\delta}\sin(\omega\delta)\ , \quad (2b)$$

where θ and δ are the durations of the 388.9-nm dye-laser pulse and Nd:YAG-laser pulses, respectively, and $\tau=\theta+\delta$. Phase shifts arising from the odd part of the signal[7,8] are discussed below.

The function $\omega(B)$, the frequency difference between the $J=2$, $M=2$, and $J=M=0$ sublevels, is very nearly linear in a 0.0007-T range centered at about 0.2277 T. We calculated $\omega'(B-B_0)=\omega(B)$ by using the best previously obtained values of the fine-structure splitting as input parameters to a simple diagonalization of the helium Zeeman Hamiltonian. Here B_0 is a fitting parameter corresponding to the crossing position. The results of this calculation are only weakly dependent on the input fine-structure splitting, which consequently has negligible effect on the calculation of $\omega(B)$ and the subsequent fit of Eq. (1) to the data. This nonlinear least-squares fit has five free parameters, one of which is the channel number at the center of the signal. Since the NMR frequency for each of these 100 channels is very well known, we can extract the NMR frequency for the center of the signal.

A run consists of five to ten bidirectional sweeps of the field, each sweep lasting about 13 min (about 8 s or 60 laser pulses in each channel during one sweep). Data from two typical runs are shown in Fig. 5 along with the fitted curves from Eq. (1). We have 102 such runs, taken with various delays and field orientations, as discussed below. These data are summarized in Table I.

The field sweep in each run is a series of 100 discrete steps of 300 Hz of NMR, and in order to reduce various temporal effects, data is taken by sweeping the field up and then down. Each sweep therefore has a total of 200 steps and the signal from channels of corresponding field values are added. This method averages away temporal linear distortions of the signal that may arise from laser power drift, laser frequency drift, metastable source intensity drift, etc. Because these linear drifts seem almost unavoidable, this bidirectional sweeping method makes a very large improvement in the quality of the data. After each field step we veto the data from the next ten laser

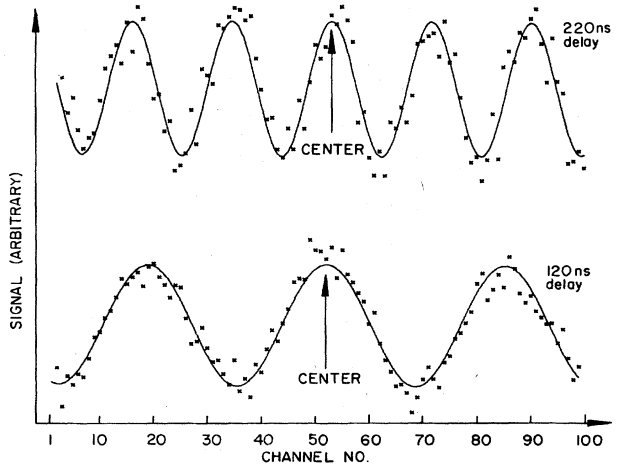

FIG. 5. Sample of data from two different delay times. Longer delay results in more inflection points for more-sensitive fitting as well as less susceptibility to effects of asymmetries and other sources of systematic errors.

TABLE I. Summary of our 102 experimental runs, as described in text.

No.	Center (Hz)	Field correction (Hz)	Delay (ns)	No.	Center (Hz)	Field correction (Hz)	Delay (ns)
1	9 695 210(76)	561.8	128	52	9 695 143(87)	609.8	119
2	9 695 096(83)	561.8	117	53	9 694 732(112)	619.8	127
3	9 695 012(65)	566.8	120	54	9 695 046(152)	603.8	73
4	9 695 160(57)	569.8	120	55	9 695 012(52)	593.8	217
5	9 695 185(83)	573.8	120	56	9 695 050(198)	583.8	77
6	9 694 927(66)	577.8	119	57	9 695 038(41)	573.8	220
7	9 694 906(64)	581.8	121	58	9 694 995(53)	563.8	208
8	9 695 073(76)	600.8	119	59	9 695 100(58)	571.8	207
9	9 695 031(63)	606.8	119	60	9 695 003(44)	576.8	211
10	9 695 021(76)	618.8	123	61	9 695 013(44)	579.0	214
11	9 695 068(72)	631.8	121	62	9 694 855(83)	579.0	211
12	9 695 039(93)	641.8	120	63	9 694 920(71)	592.0	212
13	9 695 140(100)	656.8	120	64	9 695 062(40)	600.0	209
14	9 694 785(94)	644.8	167	65	9 695 127(73)	608.0	211
15	9 694 993(52)	634.8	168	66	9 694 954(62)	617.0	212
16	9 694 837(122)	606.8	124	67	9 694 910(69)	624.0	212
17	9 694 890(80)	596.8	120	68	9 695 103(53)	611.0	211
18	9 695 027(89)	597.8	121	69	9 695 234(68)	603.0	218
19	9 694 824(75)	600.8	121	70	9 695 029(70)	595.0	209
20	9 695 075(84)	603.8	126	71	9 695 082(55)	587.0	213
21	9 694 883(90)	606.8	120	72	9 694 942(50)	579.0	212
22	9 694 540(88)	609.8	121	73	9 694 983(63)	560.0	210
23	9 694 961(68)	592.8	108	74	9 694 896(49)	552.0	212
24	9 694 761(67)	589.8	106	75	9 694 843(51)	547.0	217
25	9 695 152(93)	584.8	106	76	9 694 846(51)	540.0	217
26	9 695 004(97)	580.8	113	77	9 694 896(41)	548.0	210
27	9 694 934(111)	574.8	106	78	9 694 921(38)	555.0	350
28	9 694 844(73)	568.8	112	79	9 694 958(33)	562.0	353
29	9 695 398(70)	565.8	112	80	9 694 971(51)	567.0	216
30	9 694 835(73)	557.8	119	81	9 694 956(52)	570.0	210
31	9 694 870(91)	554.8	119	82	9 695 080(60)	570.0	210
32	9 694 876(68)	558.8	116	83	9 694 996(45)	570.0	211
33	9 695 042(76)	560.8	117	84	9 695 070(78)	1397.0	218
34	9 694 987(78)	563.8	115	85	9 694 978(47)	1348.0	214
35	9 694 928(75)	568.8	118	86	9 694 897(39)	1350.0	212
36	9 694 918(110)	571.8	114	87	9 694 924(35)	1352.0	214
37	9 694 721(96)	581.8	112	88	9 694 956(41)	1355.0	214
38	9 695 039(82)	589.8	120	89	9 695 158(64)	1379.0	216
39	9 694 903(86)	599.8	117	90	9 695 207(43)	1392.0	219
40	9 695 089(86)	609.8	117	91	9 695 101(40)	1406.0	220
41	9 694 971(120)	619.8	119	92	9 695 174(48)	1416.0	213
42	9 695 116(54)	614.8	116	93	9 694 810(45)	1406.0	217
43	9 694 927(74)	604.8	113	94	9 694 986(46)	1391.0	215
44	9 695 050(49)	586.8	114	95	9 695 075(39)	1371.0	218
45	9 695 014(65)	578.8	116	96	9 695 132(48)	1360.0	217
46	9 695 227(63)	568.8	115	97	9 694 902(55)	1372.0	218
47	9 694 848(85)	579.8	111	98	9 695 023(44)	1392.0	216
48	9 695 087(120)	586.8	121	99	9 694 999(38)	1401.0	217
49	9 695 189(117)	591.8	114	100	9 695 019(41)	1409.0	217
50	9 694 923(54)	597.8	114	101	9 695 072(80)	1480.0	218
51	9 694 852(68)	603.8	116	102	9 695 139(67)	1490.0	219

pulses in order to allow extra settling time for the field.

The center frequency from each of these 102 runs, appropriately corrected for NMR probe effects and field inhomogeneity (see below), is plotted in a histogram in Fig. 6. The standard deviation of this distribution of results is about 11 ppm, just slightly larger than the 8 ppm typical uncertainty of the center frequency returned by the fitting program. This result, along with a quite satisfactory T test of the distribution in Fig. 6, gives us confidence that the spread of the data is purely statistical, and that we can assign a statistical error of about 1.1 ppm$=$11 ppm $/\sqrt{102}$ to our measurements. This corresponds to about

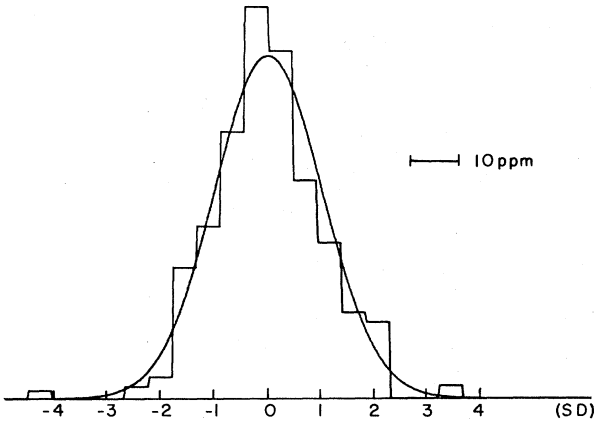

FIG. 6. Histogram of results of measurements. The standard deviation of 11 ppm is slightly larger than the 8-ppm uncertainty typically returned by the program.

0.03 channel.

The measured result from these experiments, along with its statistical uncertainty, is then $f(\text{meas})=9694.998(11)$ kHz. The diamagnetic correction results in $f(\text{corr})=9694.984(11)$ kHz. This number must be corrected for the chemical shift of the oil, and its uncertainty must be modified to account for possible systematic errors.

IV. SYSTEMATIC ERRORS

This experiment is carefully designed to minimize many sources of systematic error. It is done in the vacuum environment of an atomic beam to remove effects of collisions and discharges. There is no rf power to shift or broaden the signal. The experiment measures the phase evolution of an atom in the dark, thereby eliminating most effects of light shifts.[8] The principle systematic effects we consider are those that derive from alignment and from magnetic field measurement.

A. Alignment and asymmetry

The expression for the signal in Eq. (1) is symmetric about $\omega=0$ because the second term of Eq. (22) of Ref. 7 was left out. With exact adherence to 90° geometry for laser polarizations and magnetic field, this term is indeed zero. However, there are certain misalignments that would add a second term, proportional to another parameter C_2, that is antisymmetric about $\omega=0$. For small misalignments C_2 is small and constitutes a phase shift ϕ in the oscillations given by $\tan(\phi)=C_2/C_1$. This results in a shift of the center of the signal to a field different from that of the level crossing.

In order to minimize the effects of such a systematic error, we very carefully align the two lasers to be counterpropagating and accurately perpendicular to the z-directed magnetic field. There are two kinds of misalignments that can cause asymmetry errors. The first of these is nonparallelism of the laser beams (assuming them to be in the xy plane). Since the two laser beams are easily aligned to less than 0.002 rad, the resulting shift is only 0.62 ppm for 120-ns time delay and 0.36 ppm for 220-ns time delay. The second is misalignment of the polarization directions of two laser beams. If they are propagating parallel to one another, this misalignment causes a shift only when the propagation direction is not in the xy plane. In our experiment, the polarization misalignment is less than 5° and the laser propagation direction error is less than 2°, resulting in a shift less than 1 ppm for $T=120$ ns and 0.55 ppm for $T=220$ ns. The longer time delay makes more oscillations in the signal without increasing the phase shift, resulting in smaller errors.[6] Since much of our data is taken with 220-ns delay, and $\frac{1}{5}$ of it is taken with the field reversed, thereby reversing the sign of the shift (see below), we conclude that the systematic error expected from alignment effects is less than 0.6 ppm.

We have made two independent checks to determine an upper limit of such systematic errors. First, of the 44 runs with 220-ns delay, 19 of them were taken with the current in the main electromagnet reversed (field reversed). This changes the sign of the phase shift but not its magnitude. The difference between the center of the distribution of results of the 19 field-reversed runs [9695.044(24)] and that of the other 25 220-ns runs [9695.016(18)] is 2.9(3.1) ppm. (These numbers include both diamagnetic and chemical shift corrections to our raw data—see below.)

Second, 51 runs were taken with a 120-ns delay and field direction "normal." The difference between the center of the distribution of these [9695.020(21)] and that of the 25 220-ns runs with field normal is 0.4(2.8) ppm (also including corrections). We also have a few runs with delays of 80, 170, and 350 ns and their distributions are essentially the same as those of the other delay times, but with poorer statistics because of fewer runs. Since the magnitudes of C_1 and C_2 are independent of T, but the frequency of the oscillations is not, increasing the delay should decrease the shift caused by any terms antisymmetric in ω.[6] Since we see no well-defined shift revealed from these two tests, and since combining them puts an experimental upper limit of 0.3(2.0) ppm on this class of systematic effects, we conclude that asymmetries arising from any of several possible causes such as misalignment could shift our result by less than the 0.6 ppm estimated theoretically above.

It is also possible that light shifts caused by off-resonant effects produced during the short time of the 388.9-nm laser pulse could cause an atomic phase shift and possibly affect the results.[8] We have calculated that these should be much less than 0.1 ppm. In order to further check this possibility, we took six runs with a 6-dB attenuating filter in the laser beam. The difference between these and the other 96 was 2(6) ppm and they had about the same scatter as the rest of the data, thereby providing further evidence against such effects.

B. Field inhomogeneity and field measurement error

The diameters of the 388.9-nm dye laser and the 532-nm green laser are 2 and 6 mm, respectively (see Fig. 7).

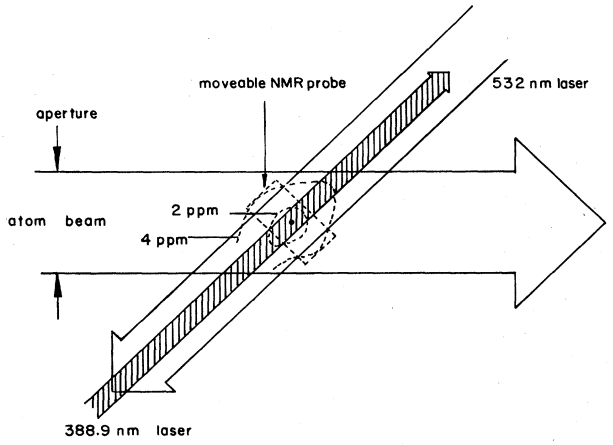

FIG. 7. Detailed geometry of interaction region showing the interaction region and the space occupied by the movable probe when it is in place. Field map is superimposed.

The diameter of an aperture placed close to the interaction region in order to define the atomic beam is 10 mm. The interaction region is therefore a 2-mm-diam by 14-mm-long cylinder. The movable NMR probe that is placed in this region for field calibration is a 3.7-mm-diam cylinder, 6-mm long, oriented perpendicular to the interaction volume defined by the laser beams. According to a map of the field of this magnet at 2277 G (Ref. 14) the inhomogeneity over this region is about 4 ppm. Since the NMR probe partially averages this inhomogeneity, we conclude that any systematic error arising from the different shape of these volumes is 20% of this or about 0.8 ppm. Because the fixed NMR probe experiences the identical conditions for either field calibration or data taking, there is no additional systematic error for the inhomogeneity where it is located. We have determined that the position of the movable probe has no measureable effect (less than 0.4 ppm) on the frequency of the fixed probe.

A small probe is moved into the interaction region in order to measure the field difference between it and the location of the fixed probe that is used for field sweeping and locking. It is placed against a mechanical stop to assure its positioning repeatability, and is carefully located to optimize its averaging over the field inhomogeneity. The typical measured field difference between the two places is 60 ppm for field normal and 140 ppm for field reversed, and has a standard deviation of about 4 ppm. We assume that any errors from this are random and only contribute to the statistical scatter of the data. This effect may be partially responsible for the difference between the 11-ppm spread of our measurements and the 8-ppm uncertainty in each of them returned by the fitting program.

The bidirectional field sweep and veto of data from the first ten laser pulses effectively cancels any problems arising from magnetic field settling errors (our check of these shows them to be very small). Of course, small dc drifts of the lock-in amplifier and associated circuits could cause error, but this kind of error changes randomly and should average to zero, causing only statistical fluctuations.

C. Stark-shift error

In the interaction region there is an electric field of about 150 V/cm used to direct the photoelectrons into the detector. In order to calculate the Stark effect of the $J=2$, $M=2$, and $J=M=0$ sublevels caused by this electric field we use hydrogenic wave functions and consider only contributions caused by mixing with the triplet S and D states having $n=3$–5.[15] We find that 150 V/cm only causes a 0.11-ppm shift of the crossing position. The motional electric field is negligible.

D. Detector gain constancy

The gain of the MCP depends mainly on the bias voltage applied to it, but it varies slightly with magnetic field. Since the field sweep in this experiment is only 7×10^{-4} T at 0.227 T, this effect is very small. In our experiment, there is some small background signal that may be derived from either ultraviolet light produced when metastables strike the metal surfaces near the interaction region or collisions with residual gas atoms in the 10^{-6}-Torr vacuum. This is present with the lasers off. We measure the magnitude of this background versus the field in order to determine the field dependence of the MCP gain. After averaging a series of 20 sweeps, we find that the normalized MCP gain is $1.0+2.7\times10^{-5}N$, where N is the channel number that ranges from 1 to 100. This small effect can shift our result by no more than 0.1 ppm.

E. Fitting program

We have tested the fitting program by giving it different starting points and using different mesh sizes for fitting the same set of data. This test was repeated with a few of the data sets, and the effects were insignificant. We conclude that error arising from the fitting program are less than 0.1 ppm. All these contributions to the systematic error are summarized in Table II. Their quadratic sum is 1.0 ppm.

V. RESULTS AND CONCLUSIONS

Our final measured result of magnetic field crossing point in units of NMR frequency in oil is f(corr) $=9694.984(15)$ kHz. The uncertainty is the result of quadrature combination of the contributions from the systematic errors summarized in Table II and the statistical uncertainty of 1.1 ppm discussed earlier. In order to compare this with other measurements, usually measured with water-filled probes, we correct it by the chemical shift difference between oil and water. This correction is about 3.9(6) ppm resulting in f(water)$=9695.023(16)$ kHz.[16] We

TABLE II. Systematic errors.

Alignment asymmetry	0.6 ppm
Light shift	0.1 ppm
Inhomogeneity averaging	0.8 ppm
Stark shift	0.1 ppm
Detector gain	0.1 ppm
Fitting program	0.1 ppm

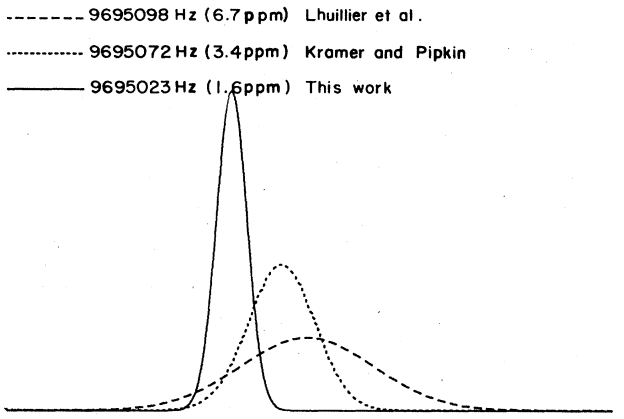

FIG. 8. Comparison of this result with the previously published work. There is good agreement among all measurements but the present work is the most precise one.

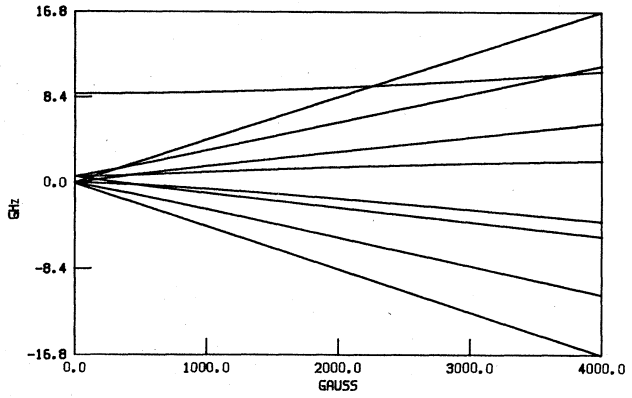

FIG. 9. Zeeman levels of $3\,^3P$ helium. The $(J,M)=(2,2)$ and (0,0) crossing is at about 2277 G. The $(J,M)=(1,1)$ and (0,0) crossing is at about 3700 G.

find good agreement with the results of Kramer and Pipkin,[5] Lhuillier *et al.*,[4] and Kaul.[3] The result is also in good agreement with our earlier work.[1] These comparisons are summarized in Fig. 8 which clearly shows the improvement that results from this work.

To determine the $3\,^3P$ helium fine-structure splittings the single level-crossing position measurement reported here is not sufficient (see Fig. 9). We plan to measure the level crossing between the $J=1$, $M=1$, and $J=M=0$ sublevels near 0.37 T (using different geometry to allow detection). We also plan a more detailed Zeeman-effect calculation in order to extract a better value for the fine-structure splittings in this state from these two independent Zeeman level-crossing measurements. We expect it will be far more precise than the current theoretical result,[2,17] and that it will provide the motivation for further work in both theory and experiment.

ACKNOWLEDGMENTS

We acknowledge the early work on this apparatus by Mark Feldman, and help from T. Breeden, L. DiMauro, and T. Q. Dong. We also wish to thank Pat McNicholl for many enlightening discussions. This work was supported in the early stages by a Precision Measurements Grant from the National Bureau of Standards, and currently by the National Science Foundation.

[1] M. Feldman *et al.*, in *Precision Measurements and Fundamental Constants II,* Natl. Bur. Stand. (U.S.) Spec. Publ. No. 617, edited by W. Phillips and B. Taylor (U.S. GPO, Washington, D.C., 1984), p. 153; T. Breeden *et al.*, Bull. Am. Phys. Soc. **26**, 22 (1981); M. Feldman and H. Metcalf, *ibid.* **25**, 493 (1980).

[2] W. Frieze *et al.*, in *Precision Measurements and Fundamental Constants II,* Natl. Bur. Stand. (U.S.) Spec. Publ. No. 617, edited by W. Phillips and B. Taylor (U.S. GPO, Washington, D.C., 1984), p. 149.

[3] R. D. Kaul, J. Opt. Soc. Am. **57**, 1156 (1967).

[4] C. Lhuillier, J-P. Faroux, and N. Billy, J. Phys. (Paris) **37**, 335 (1976); C. Lhuillier, P. Riviere, and J-P. Faroux, C. R. Acad. Sci. B **276**, 607 (1973).

[5] P. Kramer and F. Pipkin, Phys. Rev. A **18**, 212 (1978).

[6] H. Metcalf and W. Phillips, Appl. Opt. **5**, 540 (1980); W. Phillips and H. Metcalf, in *Precision Measurements and Fundamental Constants II,* Natl. Bur. Stand. (U.S.) Spec. Publ. No. 617, edited by W. Phillips and B. Taylor (U.S. GPO, Washington, D.C., 1984), p. 177.

[7] F. Raab, T. Bergeman, D. Lieberman, and H. Metcalf, Phys. Rev. A **24**, 3120 (1981).

[8] T. Q. Dong and H. Metcalf, Phys. Rev. A **25**, 3435 (1982).

[9] C. Otis and P. Johnson, Rev. Sci. Instrum. **51**, 1128 (1980).

[10] M. Feldman, P. Lebow, F. Raab, and H. Metcalf, Appl. Opt. **17**, 774 (1978).

[11] D. H. Yang, T. Breeden, and H. Metcalf, Appl. Opt. **24**, 1899 (1985).

[12] E. R. Andrew, *Nuclear Magnetic Resonance* (Cambridge University, Cambridge, England, 1955), p. 78.

[13] T. S. Luk, L. Di Mauro, and H. Metcalf, Phys. Rev. A **24**, 864 (1981).

[14] M. Feldman, Ph.D. thesis, State University of New York at Stony Brook, 1980.

[15] H. Bethe and E. Salpeter, *Quantum Mechanics of One- and Two-Electron Atoms* (Plenum, New York, 1977), p. 242.

[16] W. Phillips, W. Cooke, and D. Kleppner, Phys. Rev. Lett. **35**, 1619 (1975); B. Taylor, W. Parker, and D. Langenberg, Rev. Mod. Phys. **41**, 375 (1969).

[17] Y. Accad, C. L. Pekeris, and B. Schiff, Phys. Rev. A **4**, 516 (1971).